Rekola, Heikki T.; Hakala, Tommi K.; Törmä, Päivi

One-Dimensional Plasmonic Nanoparticle Chain Lasers

Published in:
ACS Photonics

DOI:
10.1021/acsphotonics.8b00001

Published: 16/05/2018

Document Version
Peer reviewed version

Please cite the original version:
Rekola, H. T., Hakala, T. K., & Törmä, P. (2018). One-Dimensional Plasmonic Nanoparticle Chain Lasers. *ACS Photonics*, *5*(5), 1822-1826. https://doi.org/10.1021/acsphotonics.8b00001

One-dimensional plasmonic nanoparticle chain lasers

Heikki T. Rekola,* Tommi K. Hakala, and Päivi Törmä*

Department of Applied Physics, School of Science, Aalto University, Espoo, Finland

E-mail: heikki.rekola@gmail.com; paivi.torma@aalto.fi

Abstract

Controlling and generating coherent light fields in the nanoscale is critical for reducing the size of photonic circuitry. There are several demonstrations of zero, one, two and three dimensional nanolaser architectures. Here we experimentally demonstrate a one dimensional plasmonic laser, which consists of a periodic chain of aluminum nanoparticles and organic gain media. Lasing is observed at visible wavelengths, with clear thresholds and linewidths down to 0.11 nm. Lasing occurs in a dark mode which extends over the whole structure, even outside the pumped area. The single lithography step fabrication and one dimensional character allow for easy integration of these laser sources with other plasmonic structures.

Keywords

Plasmonics, nanolasers, aluminum nanoparticles, surface lattice resonances, plasmonic crystals

Bringing the size of laser sources of light to the nanoscale holds promise for new technological applications in integrated photonic circuits.[1] Traditional laser sources relying on the

refractive index contrast between dielectric materials limit the mode volumes to the order of $(\lambda/(2n))^3$.[2] A way around this limitation is to use surface plasmon resonances found in metallic nanostructures.[3,4] Truly nanoscale laser light sources such as spasers[5] and stopped-light points in layered structures[6] have been proposed. In addition, there exists a wealth of experimental demonstrations of plasmonic nanoscale lasers where the size of the structure exceeds 100 nm in size in only one or two dimensions (1D or 2D). Planar (2D) periodic plasmonic laser structures, such as nanoparticle arrays[7,8] and nanohole arrays[9] confine the field with the plasmonic resonances in the out-of-plane direction, without the need for total internal reflection that is present in 2D photonic crystal lasers.[2] Analogs of traditional laser cavities have been formed on metal surfaces by utilizing surface plasmon polaritons (SPPs) propagating on the metal-dielectric interface.[10]

One dimensional (1D) plasmonic lasers further confine the fields in the transverse directions to propagation. Metal-insulator-semiconductor cavities with semiconductor nanowires[11,12] are one of the most studied plasmonic laser types, with demonstrations of lasing from the telecom[13] to the ultraviolet wavelengths,[14] with ultrafast dynamics.[15] Much of the progress has come from material optimization, for instance through epitaxially grown metal films.[16] Coupling the semiconductor nanowires directly into plasmonic waveguides[17] is required for integrating the lasers into full photonic circuits.[18] One major drawback of this system is the lack of control over the lasing wavelength, which is mainly determined by the size and material of the semiconductor nanowire. Other types of 1D plasmonic lasers include silver nanowires surrounded by gain medium[19] and distributed feedback lasers on plasmonic waveguides.[20] A line of densely packed silver nanoparticles on top of a laser crystal has been used to assist in lasing.[21]

In this letter we introduce a new type of a 1D plasmonic laser based on a periodic chain of aluminum nanoparticles, covered with organic dye molecules as the gain medium. The lasing frequency is controlled through the nanoparticle spacing. While the plasmonic resonances in individual aluminum nanoparticles are broad, when arranged in a periodic array significant

linewidth narrowing has been observed.[22] The lasing mechanism and the optical modes found in the nanoparticle chains are closely related to the ones found in 2D arrays of nanoparticles, and we will use 2D square arrays as the higher dimensional comparison to the 1D chains throughout this letter.

Results and discussion

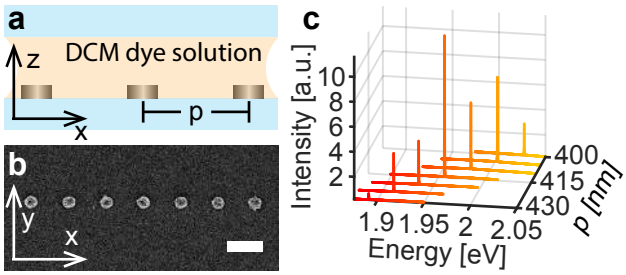

Figure 1: Schematic of a side view of the studied structure (a), and a scanning electron micrograph (SEM) top view of a typical fabricated sample (b). The scale bar in (b) is 400 nm. Chains made from cylindrical aluminum nanoparticles with varying periods p were fabricated using electron beam lithography on glass substrates. The particle diameter is 120 nm, and the height is 50 nm. A drop of 40 mM solution of DCM molecules is then added on top of the chains as the organic gain medium, with a second glass slide to contain the fluid. The lasing emission spectra just above the lasing threshold are shown in (c). The period p is varied in 5 nm steps from 430 nm to 400 nm in (c).

One-dimensional chains of aluminum nanoparticles were fabricated using electron beam lithography on glass substrates (see Experimental for details). A schematic side view of the sample structure is shown in Figure 1 (a) and a scanning electron micrograph top view in (b). The spacing between neighboring particles, p, defines the periodicity of the structure. Square arrays with the same nominal particle size and periodicities were fabricated for comparison. As the gain material, a drop of 40 mM solution of 4-(Dicyanomethylene)-2-methyl-6-(4-dimethylaminostyryl)-4H-pyran (DCM) laser dye is placed between the glass substrate and a cover glass, resulting in an approximately 6 μm thick dye layer.

The fabricated structures are pumped using a 450 nm, 100 fs output from an optical parametric amplifier with a repetition rate of 1 kHz. The pump wavelength is close to the

plasmon resonance of the aluminum nanoparticles and the absorption peak of the DCM molecules. The light emitted by the sample is collected with a 10x magnification, 0.3 NA microscope objective for measuring both the angle-resolved (Fourier-space) and spatially resolved (real-space) spectra. Emission spectra just above the lasing threshold are shown for single chains with periodicities between 400 nm and 430 nm in Figure 1 (c), showing adjustability of the emission wavelength over a 45 nm bandwidth.

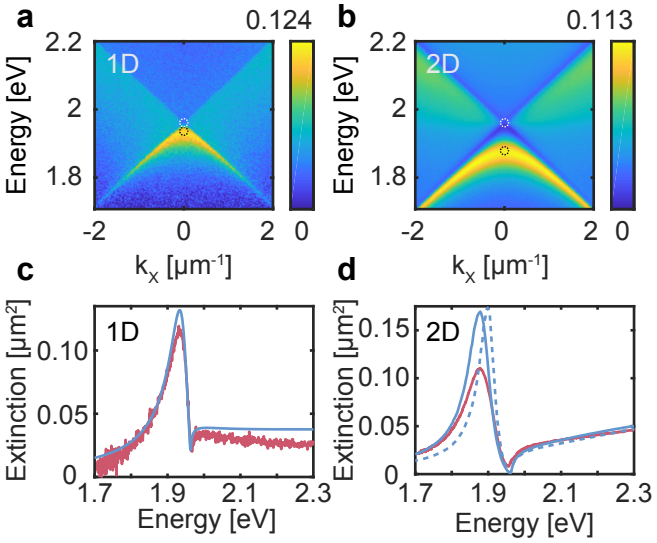

Figure 2: Optical properties of the 1D chains and 2D arrays of nanoparticles with a period p of 415 nm. The experimentally measured dispersion relations of a 1D chain is in (a), and of a 2D square array is in (b). The electric field is polarized along the y-direction (TE-polarization). At the Γ-point ($k_x = 0$) there are two SLR resonances, a bright mode and a dark mode,[8] marked with black and white circles, respectively. The measured extinction cross sections at the Γ-point are shown as red lines in (c) and (d) for the 1D and 2D structures, respectively. The blue lines in (c) and (d) are simulated spectra with 114 nm particle diameter in (c), and 114 nm (dashed line) and 120 nm (solid line) in (d). An excellent match is found between the simulation and experiment for the 1D chains. For the 2D array, the peak location matches between the experiment and the simulation with 120 nm particles, but with lower peak amplitude in the experiment.

We will focus on structures with 415 nm periodicity for the rest of this letter. Both the 1D nanoparticle chains and 2D arrays support surface lattice resonances (SLRs), which are a combination of diffracted orders (DOs) propagating along the structure, and the localized surface plasmon resonances (LSPRs) of the nanoparticles.[23] The experimentally measured TE-polarized dispersion relations for the 1D and 2D structures are shown in Figure 2 (a) and

(b), respectively. For the TE-polarized dispersions the wave vector is along the x-direction, and the electric field is along the y-direction. Due to the large losses in the SLR modes, the finite sizes of the measured structures does not play a significant role in the extinction measurements. With optical gain, the losses in the SLR modes can be compensated for, and the finite size of the structures becomes visible in the laser emission characteristics.[8]

For the 1D chain in Figure 2 (a) the SLR dispersion follows closely the linear dispersion of the DOs, with only a slight redshift at the Γ-point ($k_x = 0$) due to coupling of the two crossing modes. In contrast, the SLR dispersion for the 2D structure shown in Figure 2 (b) has a much more noticeable redshift at the Γ-point due to stronger coupling. This coupling strength is the main difference between the 1D nanoparticle chain and the 2D rectangular nanoparticle lattices when looking at the TE-polarized dispersion.

The 1D chain can be taken as the limiting case for a 2D array, with an infinite y-period. When this period in y is decreased, light scattered by the particles becomes more directional in the x-z plane, leading to the stronger coupling observed in the k_x-direction of the 2D array. The full 2D array dispersion[24] is a function of both k_x and k_y, where Figure 2 (b) shows only a cross section of it at $k_y = 0$. For the 1D chains, the SLR modes are only seen when the electric field is perpendicular to the chain ($E \perp x$), and the dispersion is a function of only k_x. We will show how this difference in dispersions affects the laser emission patterns of the two structures.

The extinction spectra at the Γ-point are shown in Figure 2 (c) and (d), together with coupled dipole approximation (CDA) simulations[25] (see Supporting information for details). The SLR resonance of the 2D structure is redshifted by 64 meV compared to the 1D chain, and it has a larger full width at half maximum (FWHM) of 95 meV compared to 72 meV. The match between the simulations and experiments is excellent for the 1D chains when a particle diameter of 114 nm is used. For the 2D arrays, the peak position matches well with 120 nm particles, however the experimentally observed peak amplitude is lower, leading to a larger FWHM. The simulated 2D array has a FWHM of 66 meV.

The real-space emission spectrum from a single 1D chain is shown in Figure 3 (b)-(d) below, at, and above the lasing threshold. Figure 3 (a) shows a schematic of the experiment. The dye molecules are pumped only in the center portion of the nanoparticle chain, leading to a strong spontaneous emission in the region visible in Figure 3 (b) and (c). When the lasing threshold is reached in Figure 3 (c), a nonlinear increase in the emission intensity at a single energy can be seen across the whole nanoparticle chain, even outside the pumped area. Above the lasing threshold (Figure 3 (d)) the laser output dominates the measured signal, with the maximum output intensity at the edges of the pumped area. This is similar to the real-space intensity pattern observed for the dark mode lasing in 2D nanoparticle arrays,[8] suggesting that the dark SLR mode has the lowest lasing threshold in the studied system. The bright SLR mode can be seen to lase in structures made with smaller nanoparticles (see Supporting information).

The output power, linewidth and laser emission peak positions are shown in Figure 3 (e) and (f). The characteristics of a single nanoparticle chain are compared to a 2D square array with the same period and nominal particle size. The single nanoparticle chain performs remarkably close to its 2D counterpart, with a threshold of 0.219 mJ/cm^2 compared to 0.161 mJ/cm^2 for the 2D array. The output linewidth is narrower compared to the 2D array at equal pump powers, however at the lasing threshold the 2D array has a linewidth of 0.27 meV (0.09 nm) and the 1D chain has a linewidth of 0.35 meV (0.11 nm). The emission peak linewidth and position below the lasing threshold could not be determined for the 1D chain due to the strong spontaneous emission background. With the 2D array, the bright SLR mode of the lattice can be seen below the lasing threshold, with a linewidth of 23 meV, at around 1.956 eV. Above threshold, the dark SLR mode at 1.958 eV becomes dominant in the emission spectrum.

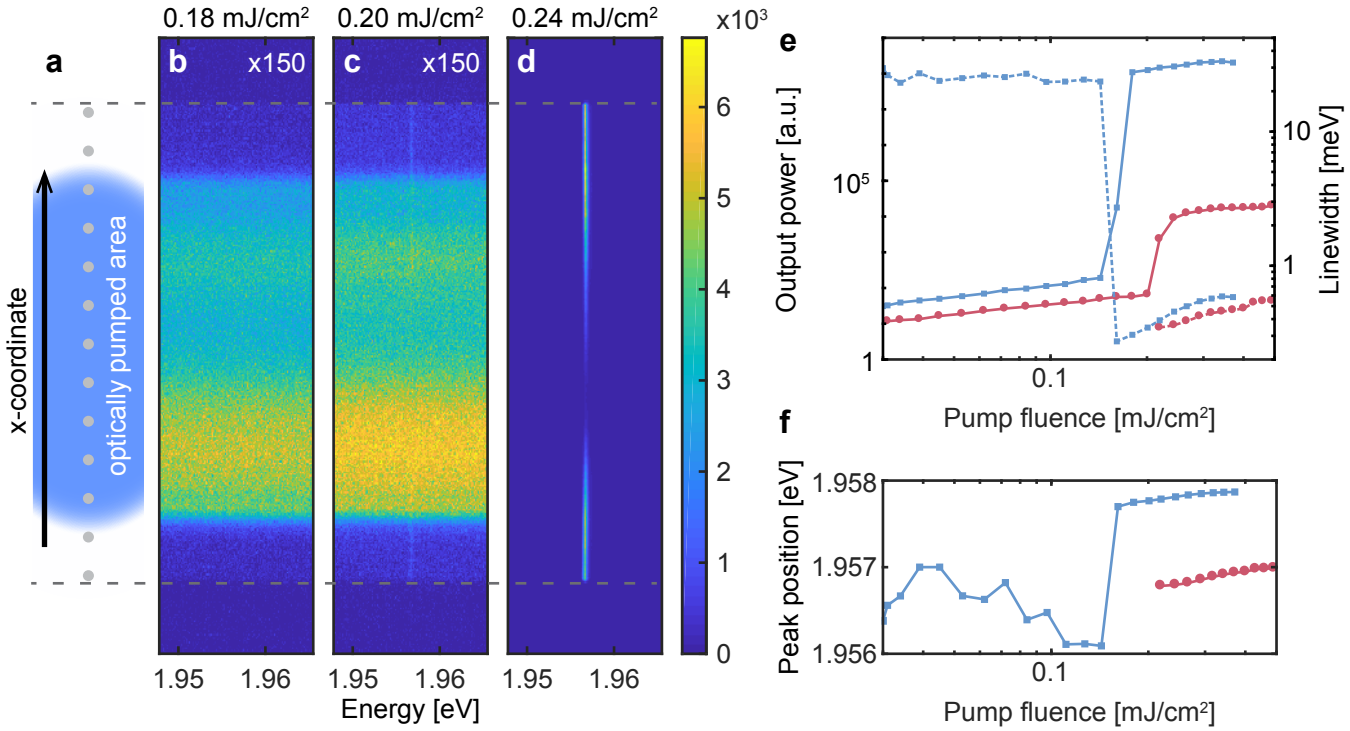

Figure 3: Schematic of the experiment (a). The emission spectrum is measured as a function of position along the 1D chain, which is optically pumped only in the center. The total length of the structure is 300 μm (indicated by the gray dashed lines). Panels (b), (c), and (d) show the position resolved emission spectra. Below the lasing threshold (b), light coupled to the nanoparticle chain can be only seen as a very faint increase in the emission intensity away from the optically pumped region. At the lasing threshold (c), emission extending over the whole 1D chain can be seen at 1.958 eV. Above the lasing threshold (d), the intensity of the lasing mode outweighs the spontaneous emission background in the measurement. In panel (e), the power dependence of the 1D chain (red lines) is compared to a 2D square array with the same periodicity and nominal particle size (blue lines). The power dependence is shown with solid lines, while dashed lines are used for the linewidth. The emission peak positions are shown in panel (f).

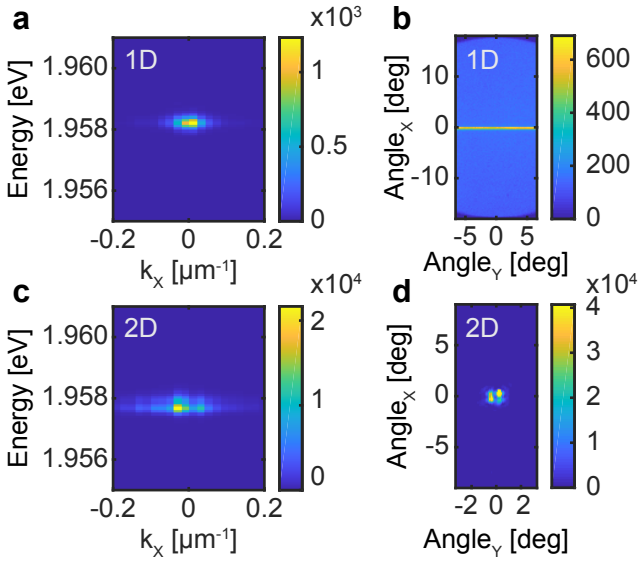

Figure 4: Fourier-space characterization of the laser emission. In (a) and (c) the angle and energy resolved emission pattern are shown for the 1D chain and the 2D array, respectively. The polarization is in the y-direction for the 1D chains, the 2D array measurements contain both x and y polarization directions. In (b) and (d) the direct Fourier-space image of the lasing emission pattern are shown for the 1D and 2D structures. Laser emission from the 1D chain can scatter in any direction inside the yz-plane, leading to tight confinement only in the x-axis of (b). The laser emission from the 2D array has more directionality, with emission only in the normal direction to the array plane.

Both the 1D and 2D structures lase in the dark SLR mode, which can be seen when the dispersions of the emitted light in Figure 4 (a) and (c) are compared to the measured extinctions in Figure 2 (a) and (b). The dark mode is located in energy close to the crossing point of the uncoupled diffraction orders (see the white circles in Figure 2). The dark mode couples only weakly to the far-field in finite-sized array structures,[8] making it the preferred mode for lasing due to reduced radiative losses. The increased confinement in k_x seen for the 1D chain in Figure 4 (a) is due to its longer length of 300 μm, compared to 150 μm for the 2D array in Figure 4 (c).

The main difference between the 1D and 2D structures is in the directionality of the laser emission. Fourier-space images of the laser emission pattern are shown for the 1D chain and the 2D array in Figure 4 (b) and (d), respectively. The 1D chain shows narrow beam divergence only in the x-direction (along the chain). In the y-direction there is no

confinement, and the 1D chain acts as a coherent line source of radiation. The 2D array laser emits only in the normal direction to the structure (Figure 2 (f)), acting as a coherent plane source of light. The four spots in Figure 4 are due to the phase differences across the 2D array for the dark SLR mode, which leads to destructive interference at $k_x = 0$, and at $k_y = 0$. The electric field profiles for the 1D and 2D dark modes are presented in the Supporting Information, along with the real-space image of the 2D array dark SLR mode.

The optical properties of the 1D nanoparticle chains are very close to the 2D square nanoparticle lattices. Similar 1D structures have been studied by dark-field microscopy,[26] where a qualitative match between the experiment and CDA calculations was reached. We found that the 1D chains had smaller resonance linewidths in the experiment when compared to 2D arrays, similar to the early predictions made for silver nanoparticles.[25] In the numerical calculations this was not reproduced, with the 2D arrays having narrower resonances. The difference in the numerical results presented here and in Ref. 25 can originate from the size of the structures considered. A sufficiently large lattice structure is required to have narrow linewidths for the SLR modes.[27]

Compared to the semiconductor nanowire based 1D plasmonic lasers, the 1D chains can have much more directional output. At the end of a chain, the diffracted order propagating along the structure in the SLR mode will continue to propagate forward. This makes the 1D chains an ideal on-chip light source, which can be lithographically placed on the same chip as other plasmonic structures where light with a well defined wave vector and energy is needed. The dark SLR mode is ideally suited for this, as scattering to the far-field along the 1D chain is minimized.

The dimensionality of the underlying optical modes in the 2D arrays is an important question in light of the recent experiments showing Bose-Einstein condensation (BEC) of photons in similar plasmonic lattices.[28] Moving forward, it is crucial to know whether the SLR excitations in 2D arrays correspond to a single 1D optical mode, or a collection of coupled 1D modes, or truly 2D excitations. By studying the 1D sub-unit of the more

complex 2D structures, we can learn more about the underlying nature of the SLR modes, with higher control and detail than what is possible with the 2D arrays.

Experimental

Standard electron beam lithography was used for patterning the nanoparticle chain and array structures on borosilicate glass substrates using poly(methyl methacrylate) resist. The length of the nanoparticle chains is 300 μm, while the array structures are 150 $\times$ 150 μm^2. Periods between 400 nm to 430 nm are fabricated in 5 nm steps, with a nominal particle size of 120 nm. Aluminum was deposited in an e-beam evaporator under 1e-7 mBar vacuum with a fast growth rate of 1 nm/s. After the evaporation lift-off of the metal film on top of the resist was done using acetone to reveal the nanoparticle arrays and chains. The sample is then rinsed with methanol, dried with nitrogen and stored in ambient conditions prior to the measurements. 4-(Dicyanomethylene)-2-methyl-6-(4-dimethylaminostyryl)-4H-pyran laser dye (98% dye content), anhydrous benzyl alcohol ($\geq$99.8%), anhydrous dimethyl sulfoxide ($\geq$99.9%) were used for the gain medium. All chemicals were used as received and purchased from Sigma-Aldrich. The benzyl alcohol and dimethyl sulfoxide were mixed to match the refractive index of the substrate glass.[29] 40 mM of the dye was then dissolved in the solvent solution, and a small amount of aggregates were filtered out using a 0.1 μm syringe filter.

Detailed descriptions of the measurements and simulation methods can be found in the Supporting information.

Acknowledgement

This work was supported by the Academy of Finland through its Centres of Excellence Program (2012–2017) and under project NOs. 284621, 303351 and 307419, and by the European Research Council (ERC-2013-AdG-340748-CODE). Part of the research was conducted using

the OtaNano research infrastructure at the Micronova Nanofabrication Centre and at the Aalto University Nanomicroscopy Center.

Supporting Information Available

Supporting Information Available: Description of the simulation methods used, calculated electric field profiles, measurements with smaller nanoparticle diameter and characterization of the dye molecules. This material is available free of charge via the Internet at http://pubs.acs.org

References

(1) Fang, Y.; Sun, M. Nanoplasmonic waveguides: towards applications in integrated nanophotonic circuits. *Light: Science & Applications* **2015**, *4*, e294.

(2) Hill, M. T.; Gather, M. C. Advances in small lasers. *Nat. Photonics* **2014**, *8*, 908–918.

(3) Ma, R.-M.; Oulton, R. F.; Sorger, V. J.; Zhang, X. Plasmon lasers: coherent light source at molecular scales. *Laser Photonics Rev.* **2013**, *7*, 1–21.

(4) Wang, D.; Wang, W.; Knudson, M. P.; Schatz, G. C.; Odom, T. W. Structural Engineering in Plasmon Nanolasers. *Chem. Rev.* **2017**, doi:10.1021/cas.chemrev.7b00424.

(5) Bergman, D. J.; Stockman, M. I. Surface plasmon amplification by stimulated emission of radiation: quantum generation of coherent surface plasmons in nanosystems. *Phys. Rev. Lett.* **2003**, *90*, 027402.

(6) Pickering, T.; Hamm, J. M.; Page, A. F.; Wuestner, S.; Hess, O. Cavity-free plasmonic nanolasing enabled by dispersionless stopped light. *Nat. Commun.* **2014**, *5*, 4972.

(7) Zhou, W.; Dridi, M.; Suh, J. Y.; Kim, C. H.; Co, D. T.; Wasielewski, M. R.; Schatz, G. C.; Odom, T. W. Lasing action in strongly coupled plasmonic nanocavity arrays. *Nat. Nanotechnol.* **2013**, *8*, 506–511.

(8) Hakala, T. K.; Rekola, H. T.; Väkeväinen, A. I.; Martikainen, J.-P.; Nečada, M.; Moilanen, A. J.; Törmä, P. Lasing in dark and bright modes of a finite-sized plasmonic lattice. *Nat. Commun.* **2017**, *8*, 13687.

(9) van Beijnum, F.; van Veldhoven, P. J.; Geluk, E. J.; de Dood, M. J. A.; 't Hooft, G. W.; van Exter, M. P. Surface Plasmon Lasing Observed in Metal Hole Arrays. *Phys. Rev. Lett.* **2013**, *110*, 206802.

(10) Kress, S. J. P.; Cui, J.; Rohner, P.; Kim, D. K.; Antolinez, F. V.; Zaininger, K.-A.; Jayanti, S. V.; Richner, P.; McPeak, K. M.; Poulikakos, D.; Norris, D. J. A customizable class of colloidal-quantum-dot spasers and plasmonic amplifiers. *Sci Adv* **2017**, *3*, e1700688.

(11) Gwo, S.; Shih, C.-K. Semiconductor plasmonic nanolasers: current status and perspectives. *Rep. Prog. Phys.* **2016**, *79*, 086501.

(12) Oulton, R. F.; Sorger, V. J.; Zentgraf, T.; Ma, R.-M.; Gladden, C.; Dai, L.; Bartal, G.; Zhang, X. Plasmon lasers at deep subwavelength scale. *Nature* **2009**, *461*, 629–632.

(13) Lee, C.-J.; Yeh, H.; Cheng, F.; Su, P.-H.; Her, T.-H.; Chen, Y.-C.; Wang, C.-Y.; Gwo, S.; Bank, S. R.; Shih, C.-K.; Chang, W.-H. Low-Threshold Plasmonic Lasers on a Single-Crystalline Epitaxial Silver Platform at Telecom Wavelength. *ACS Photonics* **2017**, *4*, 1431–1439.

(14) Zhang, Q.; Li, G.; Liu, X.; Qian, F.; Li, Y.; Sum, T. C.; Lieber, C. M.; Xiong, Q. A room temperature low-threshold ultraviolet plasmonic nanolaser. *Nat. Commun.* **2014**, *5*, 4953.

(15) Sidiropoulos, T. P. H.; Röder, R.; Geburt, S.; Hess, O.; Maier, S. A.; Ronning, C.; Oulton, R. F. Ultrafast plasmonic nanowire lasers near the surface plasmon frequency. *Nat. Phys.* **2014**, *10*, 870–876.

(16) Lu, Y.-J.; Kim, J.; Chen, H.-Y.; Wu, C.; Dabidian, N.; Sanders, C. E.; Wang, C.-Y.; Lu, M.-Y.; Li, B.-H.; Qiu, X.; Chang, W.-H.; Chen, L.-J.; Shvets, G.; Shih, C.-K.; Gwo, S. Plasmonic nanolaser using epitaxially grown silver film. *Science* **2012**, *337*, 450–453.

(17) Bermúdez-Ureña, E.; Tutuncuoglu, G.; Cuerda, J.; Smith, C. L. C.; Bravo-Abad, J.; Bozhevolnyi, S. I.; Fontcuberta i Morral, A.; García-Vidal, F. J.; Quidant, R. Plasmonic Waveguide-Integrated Nanowire Laser. *Nano Lett.* **2017**, *17*, 747–754.

(18) Gramotnev, D. K.; Bozhevolnyi, S. I. Plasmonics beyond the diffraction limit. *Nat. Photonics* **2010**, *4*, 83.

(19) Li, Y. J.; Lv, Y.; Zou, C.-L.; Zhang, W.; Yao, J.; Zhao, Y. S. Output Coupling of Perovskite Lasers from Embedded Nanoscale Plasmonic Waveguides. *J. Am. Chem. Soc.* **2016**, *138*, 2122–2125.

(20) Keshmarzi, E. K.; Niall Tait, R.; Berini, P. Long-range surface plasmon single-mode laser concepts. *J. Appl. Phys.* **2012**, *112*, 063115.

(21) Molina, P.; Yraola, E.; Ramírez, M. O.; Tserkezis, C.; Plaza, J. L.; Aizpurua, J.; Bravo-Abad, J.; Bausá, L. E. Plasmon-Assisted Nd(3+)-Based Solid-State Nanolaser. *Nano Lett.* **2016**, *16*, 895–899.

(22) Yang, A.; Hryn, A. J.; Bourgeois, M. R.; Lee, W.-K.; Hu, J.; Schatz, G. C.; Odom, T. W. Programmable and reversible plasmon mode engineering. *Proc. Natl. Acad. Sci. U. S. A.* **2016**, *113*, 14201–14206.

(23) Wang, W.; Ramezani, M.; Väkeväinen, A. I.; Törmä, P.; Rivas, J. G.; Odom, T. W. The rich photonic world of plasmonic nanoparticle arrays. *Mater. Today* **2017**, doi:10.1016/j.mattod.2017.09.002.

(24) Moerland, R. J.; Hakala, T. K.; Martikainen, J.-P.; Rekola, H. T.; Väkeväinen, A. I.; Törmä, P. In *Quantum Plasmonics*; Bozhevolnyi, S. I., Martin-Moreno, L., Garcia-Vidal, F., Eds.; Springer Series in Solid-State Sciences; Springer International Publishing, 2017; pp 121–150.

(25) Zou, S.; Janel, N.; Schatz, G. C. Silver nanoparticle array structures that produce remarkably narrow plasmon lineshapes. *J. Chem. Phys.* **2004**, *120*, 10871–10875.

(26) Hicks, E. M.; Zou, S.; Schatz, G. C.; Spears, K. G.; Van Duyne, R. P.; Gunnarsson, L.; Rindzevicius, T.; Kasemo, B.; Käll, M. Controlling plasmon line shapes through diffractive coupling in linear arrays of cylindrical nanoparticles fabricated by electron beam lithography. *Nano Lett.* **2005**, *5*, 1065–1070.

(27) Rodriguez, S. R. K.; Schaafsma, M. C.; Berrier, A.; Gómez Rivas, J. Collective resonances in plasmonic crystals: Size matters. *Physica B Condens. Matter* **2012**, *407*, 4081–4085.

(28) Hakala, T. K.; Moilanen, A. J.; Väkeväinen, A. I.; Guo, R.; Martikainen, J.-P.; Daskalakis, K. S.; Rekola, H. T.; Julku, A.; Törmä, P. Bose-Einstein Condensation in a Plasmonic Lattice. **2017**, arXiv:1706.01528v2 [cond–mat.quant–gas].

(29) Francesconi, R.; Bigi, A.; Rubini, K.; Comelli, F. Excess Enthalpies, Heat Capacities, Densities, Viscosities and Refractive Indices of Dimethyl Sulfoxide + Three Aryl Alcohols at 308.15 K and Atmospheric Pressure. *J. Chem. Eng. Data* **2005**, *50*, 1932–1937.

Graphical TOC Entry